

S and P-wave heavy-light mesons in lattice NRQCD

Randy Lewis

Department of Physics, University of Regina, Regina, SK, Canada S4S 0A2

R.M. Woloshyn

TRIUMF, 4004 Wesbrook Mall, Vancouver, BC, Canada V6T 2A3

(March 2000)

Abstract

The mass spectrum of S and P-wave mesons containing a single heavy quark is computed in the quenched approximation, using NRQCD up to third order in the inverse heavy quark mass expansion. Previous results found the expansion to break down near the charm quark mass for the S-wave spin splitting. The present work considers variations such as anisotropic lattices, Landau link tadpole improvement, and a highly-improved light quark action, but finds that these modifications do not enhance convergence for charmed mesons. The expansion is reasonable for bottom mesons, and is also found to be well-behaved for the P-wave charmed masses. The relative orderings among P-wave charmed and bottom mesons, and the sizes of the mass splittings, are discussed in light of experimental data and existing calculations.

I. INTRODUCTION

Calculations in QCD can be performed numerically on a discrete space-time lattice, provided the lattice spacing is small enough to accommodate all of the relevant physical distance scales. In the presence of a heavy quark the lattice spacing must be small relative to the inverse quark mass, resulting in large computational requirements, unless an appropriate "effective theory" is used. In particular, for the case of a hadron containing exactly one heavy quark, the dynamics can be expanded in powers of the inverse heavy quark mass using the well-established technique of heavy quark effective theory [1] or nonrelativistic QCD (NRQCD) [2,3]. With the heavy quark expansion, the lattice spacing can be much coarser and the computational requirements are correspondingly smaller.

In the present work, two issues will be addressed within quenched lattice NRQCD. Firstly, is the charm quark sufficiently heavy to permit the use of lattice NRQCD for charmed meson spectroscopy? Secondly, what are the mass splittings (magnitude and sign) between P-wave mesons containing a single heavy quark?

The first issue is clearly of interest due to the computational efficiency of lattice NRQCD. The heavy quark expansion is known to work well for bottom mesons [4,5], but previous research has demonstrated that it begins to break down in the vicinity of charm. [4] The present work provides an extension of this investigation by considering new simulations that incorporate a number of changes in method. For example, Ref. [4] used the fourth root of an elementary plaquette to define the tadpole improvement factor, U_0 , whereas the present work uses the mean link in Landau gauge. Since the Landau definition is advantageous in other contexts [6], including the velocity expansion for the charmonium spectrum of lattice NRQCD [7], it might be expected to improve the convergence of the heavy quark expansion for the charmed heavy-light spectrum as well. Also, the light quark was described by the Sheikholeslami-Wohlert action in Ref. [4], but the present work uses a D234 action [8] which has smaller lattice spacing errors classically. The simulations in the present work differ from those of Ref. [4] in various other ways as well, including Dirichlet versus periodic boundary conditions for light quark propagation, differing discretizations for heavy quark propagation, and the introduction of an anisotropic lattice with a smaller temporal lattice spacing than spatial spacing. Despite these modifications, the present simulations reinforce the conclusion of Ref. [4]: there is no clear indication of convergence for S-wave charmed meson masses in lattice NRQCD.

The second issue under discussion in the present work relates to the spectrum of P-wave mesons containing a single heavy quark. The relative orderings of the P-wave bottom mesons has only recently come under direct experimental scrutiny [9-13], and the complete picture is not yet clear. Meanwhile theoretical predictions differ from one another even at a qualitative level. The traditional expectation of a hydrogen-like spectrum that arises from a number of model calculations [14-18] has been questioned long ago by Schnitzer [19] and very recently by Isgur [20] and by Ebert, Galkin and Faustov [21].

The calculation is difficult within lattice QCD because the P-wave splittings are not large in comparison to the typical scale of nonperturbative QCD, and because of operator mixing for the pair of P-wave states having $J = 1$. Some previous attempts have been made [22-25]. Unfortunately, the uncertainties are often substantial, and results are not always as consistent with one another as might have been hoped. The present work represents a

further comment on this situation. In particular, the $D_2 - D_0$ and $B_2 - B_0$ mass splittings are found to be positive as in the traditional hydrogen-like ordering. The magnitudes of the splittings are consistent with a number of model calculations, but are somewhat smaller than the lattice NRQCD calculation of Ref. [24].

II. ACTION

The lattice action has three terms: gauge action, light quark action and heavy quark action. The entire action is classically and tadpole-improved with the tadpole factors, u_s and u_t , defined as the mean links in Landau gauge in a spatial and temporal direction, respectively.

The gauge field action is

$$S_G(U) = \frac{5}{3} \sum_{ps} \frac{1}{u_s^4} \left(1 - \frac{1}{3} \text{ReTr} U_{ps} \right) + \frac{1}{20u_s^6} \sum_{rs} \left(1 - \frac{1}{3} \text{ReTr} U_{rs} \right) + \frac{1}{u_s^2 u_t^2} \sum_{pt} \left(1 - \frac{1}{3} \text{ReTr} U_{pt} \right) + \frac{1}{20u_s^4 u_t^2} \sum_{rst} \left(1 - \frac{1}{3} \text{ReTr} U_{rst} \right) + \frac{1}{20u_s^2 u_t^4} \sum_{rts} \left(1 - \frac{1}{3} \text{ReTr} U_{rts} \right); \quad (1)$$

where $a_s = a_t$. The subscripts $\backslash ps$ and $\backslash rs$ denote spatial plaquettes and spatial planar 1×2 rectangles respectively. Plaquettes in the temporal-spatial planes are denoted by $\backslash pt$, while rectangles with the long side in a spatial(temporal) direction are labeled by $\backslash rst$ ($\backslash rts$). The leading classical errors of this action are quartic in lattice spacing.

For light quarks, a D234 action [8] is used with parameters set to their tadpole-improved classical values. Its leading classical errors are cubic in lattice spacing.

$$S_F(q; q; U) = \frac{4}{3} \sum_{xji} \frac{1}{u_s^2} D_{1i}(x) + \frac{1}{8u_s^2} D_{2i}(x) + \frac{4}{3} \sum_x \frac{1}{u_t} D_{1t}(x) + \frac{1}{8u_t^2} D_{2t}(x) + \frac{2}{3u_s^4} \sum_{xji < j} (x)_{ij} F_{ij}(x) + \frac{2}{3u_s^2 u_t^2} \sum_{xji} (x)_{0i} F_{0i}(x) + \sum_x (x)_{ij} (x)_{ji}; \quad (2)$$

where

$$D_{1i}(x) = (x)_{ij} (1 - u_{ij}) U_{ij}(x) (x + \hat{i}) + (x + \hat{i})_{ij} (1 + u_{ij}) U_{ij}^\dagger(x) (x); \quad (3)$$

$$D_{1t}(x) = (x)_{ij} (1 - u_{ij}) U_{ij}(x) (x + \hat{t}) + (x + \hat{t})_{ij} (1 + u_{ij}) U_{ij}^\dagger(x) (x); \quad (4)$$

$$D_{2i}(x) = (x)_{ij} (1 - u_{ij}) U_{ij}(x) U_{ij}(x + \hat{i}) + (x + \hat{i})_{ij} (1 + u_{ij}) U_{ij}^\dagger(x + \hat{i}) U_{ij}^\dagger(x) (x); \quad (5)$$

$$D_{2t}(x) = (x)_{ij} (1 - u_{ij}) U_{ij}(x) U_{ij}(x + \hat{t}) + (x + \hat{t})_{ij} (1 + u_{ij}) U_{ij}^\dagger(x + \hat{t}) U_{ij}^\dagger(x) (x); \quad (6)$$

$$gF(x) = \frac{1}{2i} \sum_{ij} (x)_{ij} \gamma_{ij} (x) - \frac{1}{3} \text{Im}(\text{Tr} U(x)); \quad (7)$$

$$\begin{aligned}
&= \frac{1}{4} \text{tr} \left[U(\mathbf{x}) U(\mathbf{x} + \hat{\mu}) U^\dagger(\mathbf{x} + \hat{\mu}) U^\dagger(\mathbf{x}) \right. \\
&\quad + U(\mathbf{x}) U^\dagger(\mathbf{x} - \hat{\mu} + \hat{\nu}) U^\dagger(\mathbf{x} - \hat{\nu}) U(\mathbf{x} - \hat{\nu}) \\
&\quad + U^\dagger(\mathbf{x} - \hat{\nu}) U^\dagger(\mathbf{x} - \hat{\mu} - \hat{\nu}) U(\mathbf{x} - \hat{\mu} - \hat{\nu}) U(\mathbf{x} - \hat{\nu}) \\
&\quad \left. + U^\dagger(\mathbf{x} - \hat{\nu}) U(\mathbf{x} - \hat{\nu}) U(\mathbf{x} + \hat{\mu} - \hat{\nu}) U^\dagger(\mathbf{x}) \right] : \quad (8)
\end{aligned}$$

The heavy quark action is NRQCD [2], which is discretized to give the following Green's function propagation:

$$G_{i+1} = \left[1 - \frac{a_t H_B}{2} \right] \left[1 - \frac{a_t H_A}{2n} \frac{U_4^\dagger}{u_t} \right]^n \left[1 - \frac{a_t H_A}{2n} \right]^n \left[1 - \frac{a_t H_B}{2} \right] G_i; \quad (9)$$

with $n = 5$ chosen for this work. Separation of the Hamiltonian into two terms, $H = H_A + H_B$, is important for ensuring stability of the discretization. For example, recall the discussion in Ref. [4] of a large nonzero vacuum expectation value for the term containing c_{10} in the Hamiltonian (see Eq. (15)). This issue will be discussed further in Sec. IV.

The following Hamiltonian, written in terms of the bare heavy quark mass M , is complete to $O(1/M^3)$ in the classical continuum limit [26]:

$$H = H_0 + H; \quad (10)$$

$$H_0 = \frac{(2)}{2M}; \quad (11)$$

$$H = H^{(1)} + H^{(2)} + H^{(3)} + O(1/M^4) \quad (12)$$

$$H^{(1)} = \frac{c_4}{u_s^4} \frac{g}{2M} \mathbf{B} + c_5 \frac{a_s^2}{24M} \mathbf{E}^2; \quad (13)$$

$$H^{(2)} = \frac{c_2}{u_s^2 u_t^2} \frac{ig}{8M^2} (\tilde{\mathbf{E}} \cdot \mathbf{E} \cdot \tilde{\mathbf{E}}) + \frac{c_3}{u_s^2 u_t^2} \frac{g}{8M^2} (\tilde{\mathbf{E}} \cdot \mathbf{E} \cdot \tilde{\mathbf{E}}) + c_6 \frac{a_s (\mathbf{E}^2)^2}{16nM^2}; \quad (14)$$

$$\begin{aligned}
H^{(3)} = & c_1 \frac{(\mathbf{E}^2)^2}{8M^3} + \frac{c_7}{u_s^4} \frac{g}{8M^3} \tilde{\mathbf{E}}^2; \quad \mathbf{B}^0 = \frac{c_9 ig^2}{8M^3} \frac{\mathbf{E} \cdot \mathbf{E}}{u_s^4 u_t^4} + \frac{\mathbf{B} \cdot \mathbf{B}}{u_s^8} \\
& \frac{c_{10} g^2}{8M^3} \frac{\mathbf{E}^2}{u_s^4 u_t^4} + \frac{\mathbf{B}^2}{u_s^8} + c_{11} \frac{a_s^2 (\mathbf{E}^2)^3}{192n^2 M^3}; \quad (15)
\end{aligned}$$

The coefficients of the Hamiltonian are chosen so the dimensionless parameters, c_i , are unity at the classical level. As will be discussed below, computations have been performed with the c_i set to unity or zero in various combinations, including separate computations at $O(1/M)$, $O(1/M^2)$ and $O(1/M^3)$ to allow discussions of convergence for the $1/M$ expansion. Throughout this work, H_0 is always placed in H_A of Eq. (9) and all of the remaining terms except the c_{10} term are only placed in H_B . The difference between having the c_{10} term in H_A or H_B will be discussed explicitly, since it has the nonzero vacuum expectation value.

A tilde on any quantity indicates that the leading discretization errors have been removed. In particular,

$$\tilde{\mathbf{E}}_i = \mathbf{F}_{4i}; \quad (16)$$

$$\tilde{\mathbf{B}}_i = \frac{1}{2} \epsilon_{ijk} \mathbf{F}_{jk}; \quad (17)$$

where [3]

$$F^{\sim}(\mathbf{x}) = \frac{5}{3}F(\mathbf{x}) - \frac{1}{6u} \left[U_i(\mathbf{x})F(\mathbf{x} + \hat{i})U^{\dagger}_i(\mathbf{x}) + U^{\dagger}_i(\mathbf{x} - \hat{i})F(\mathbf{x} - \hat{i})U_i(\mathbf{x} - \hat{i}) - (i \leftrightarrow j) \right]; \quad (18)$$

The various spatial lattice derivatives are defined as follows:

$$a_s^{-1}G(\mathbf{x}) = \frac{1}{2u_s} [U_i(\mathbf{x})G(\mathbf{x} + \hat{i}) - U^{\dagger}_i(\mathbf{x} - \hat{i})G(\mathbf{x} - \hat{i})]; \quad (19)$$

$$a_s^{-1}G^{(+)}_i(\mathbf{x}) = \frac{U_i(\mathbf{x})}{u_s} G(\mathbf{x} + \hat{i}) - G(\mathbf{x}); \quad (20)$$

$$a_s^{-1}G^{(-)}_i(\mathbf{x}) = G(\mathbf{x}) - \frac{U^{\dagger}_i(\mathbf{x} - \hat{i})}{u_s} G(\mathbf{x} - \hat{i}); \quad (21)$$

$$a_s^2 G^{(2)}_i(\mathbf{x}) = \frac{U_i(\mathbf{x})}{u_s} G(\mathbf{x} + \hat{i}) - 2G(\mathbf{x}) + \frac{U^{\dagger}_i(\mathbf{x} - \hat{i})}{u_s} G(\mathbf{x} - \hat{i}); \quad (22)$$

$$\tilde{a}_i^2 = \frac{a_s^2}{6} G^{(+)}_i(\mathbf{x}) - G^{(-)}_i(\mathbf{x}); \quad (23)$$

$$G^{(2)}_i = \sum_j G^{(2)}_{ij}; \quad (24)$$

$$\tilde{a}^{(2)} = \sum_j \frac{a_s^2}{12} G^{(4)}_{ij}; \quad (25)$$

$$G^{(4)}_i = \sum_j G^{(2)}_{ij}{}^2; \quad (26)$$

This NRQCD action has quadratic classical lattice spacing errors.

III. METHOD

All data presented here come from 2000 gauge field configurations on $10^3 \times 30$ lattices at $\beta = 2.1$ with a bare aspect ratio of $a_s = a_t = 2$. Two light quark masses are used, corresponding to $m = 0.23$ and 0.24 . Fixed time boundaries are used for the light quark propagators so they fit naturally into a heavy-light meson, since the NRQCD heavy quark propagator is also not periodic in the temporal direction.

A calculation of the string tension from these gauge field configurations provides a determination of the lattice spacings:

$$a_s = 0.202(1) \text{ fm}; \quad (27)$$

$$a_t = 0.103(1) \text{ fm}; \quad (28)$$

$$a_s = a_t = 1.96(2); \quad (29)$$

Using light quarks only, the lightest pseudoscalar and vector meson masses are easily obtained from local creation operators. By linear interpolation and extrapolation in $1/m$,

TABLE I. Heavy-light meson creation operators.

$2S+1L_J$	(\mathbf{x})
1S_0	$(0, I)$
3S_1	$(0, i)$
1P_1	$(0, \mathbf{p}_i)$
3P_0	$(0, i_i i_i i_i)$
3P_1	$(0, i_i j_i j_i i_i)$
3P_2	$(0, i_i i_i j_i j_i) \text{ or } (0, i_i j_i + j_i i_i), i \neq j$

the critical (c) and strange (s) hopping parameters and the temporal lattice spacing are found to be

$$c = 0.243025(41); \quad (30)$$

$$s = \begin{cases} 0.2344(11) \text{ from } m_\pi, \\ 0.2356(3) \text{ from } m_K, \end{cases} \quad (31)$$

$$a_t = 0.1075(23) \text{ fm from } m_\pi : \quad (32)$$

For the hopping parameters used in explicit computations, $c = 0.23$ and 0.24 , the ratio of pseudoscalar to vector meson masses is $m_\pi/m_\rho = 0.815(3)$ and $0.517(8)$ respectively.

A heavy-light meson is created by the following operator,

$$\sum_{\mathbf{x}} Q^\dagger(\mathbf{x}) (\mathbf{x}) (\mathbf{x}) q(\mathbf{x}); \quad (33)$$

where (\mathbf{x}) is given in Table I and the smearing operator is

$$(\mathbf{x}) = [1 + c_s \nabla^2]^{n_s} : \quad (34)$$

All plots shown here use $(c_s; n_s) = (0.15; 10)$ at the source and a local sink. The source is fixed at time step 4, which is a distance $3a_t$ from the lattice boundary.

Because NRQCD is an expansion in the inverse bare heavy quark mass, all meson mass differences can be obtained from correlation functions at $\mathbf{p} = \mathbf{0}$, but the absolute meson mass itself cannot be obtained directly. One way to determine the mass is to compute the change in energy when a meson is boosted,

$$E_p - E_0 = \frac{\mathbf{p}^2}{2M_{\text{kin}}} : \quad (35)$$

This defines the kinetic mass, M_{kin} , which is interpreted as the meson's physical mass. For the present work, E_p is computed only for the 1S_0 state, with $\mathbf{p} = (0; 0; 2\pi/L_s)$ where $L_s = N_s a_s$ is the spatial extent of the lattice in physical units. Solving for the kinetic mass gives

$$M_{\text{kin}} = \frac{2\pi^2}{N_s^2 a_t^2 [a_t (E_p - E_0)]} : \quad (36)$$

For all heavy-light mesons to be discussed below, statistical uncertainties come from the analysis of 5000 bootstrap ensembles.

In the case of S-wave mesons, a plateau containing ample timesteps is clearly evident in all effective mass plots; some examples are shown in Fig. 1. In this paper, the S-wave plateau region for each mass is defined by the maximum value of

$$Q = \frac{(N=2, 1; \beta^2=2)}{(N=2, 1; 0)} \quad (37)$$

where

$$(a; x) = \sum_x \int_{t_1}^{t_2} dt t^{a-1} \exp(-t); \quad (38)$$

$$\beta^2 = \sum_t \frac{E(t) - E}{E(t)}; \quad (39)$$

$$E = \sum_t \frac{E(t)}{[E(t)]^2}, \quad \sum_t \frac{1}{[E(t)]^2}; \quad (40)$$

$E(t) - E$ denotes the simulation energy at timestep t with its bootstrap error, and sum is run over all of the N timesteps in the proposed plateau region. All plateaus are ended at timestep 22 (20) for simulations with $\beta = 0.23$ (0.24). In each case, the condition of maximum Q identifies the plateau's onset at timestep 11, 12, 13 or 14. Having identified the preferred plateau, the simulation energy is computed by fitting the correlation function to a single exponential.

The P-wave spectrum has also been analyzed in this way, although the beginning and ending timesteps for the plateaus are different. A more detailed discussion of the P-wave plateaus is deferred to Sec. V.

IV. S-WAVE SPECTRUM

Calculations were performed for $a_s M = 1.2, 1.5, 5, 6$ and 1 , where M represents the bare heavy quark mass in the NRQCD action. Figure 2 shows the simulation energy of the ground state as a function of $a_s M$ for $\beta = 0.24$. The huge $O(1=M^3)$ effect at smaller M values is due to the vacuum expectation value of the c_{10} term. This large correction to the unphysical simulation energy does not discredit the convergence of NRQCD, but special care must be taken to ensure that the large vacuum value is incorporated into the heavy quark propagation appropriately. In particular, previous work [4] has shown the linear approximation to be insufficient for the c_{10} term, which contains the vacuum expectation value, in computations of the S-wave spin splitting in the charm region. Fig. 2 explicitly shows the error introduced by placing the c_{10} term in H_B rather than H_A in Eq. (9).

It will also be noted from Fig. 2 that the simulation energy is negative for $a_s M = 1.2$ at third order in NRQCD. Of course the absolute energy scale is unphysical in NRQCD due to omission of the large heavy quark mass term from the leading order action, and physical quantities (i.e. mass differences) are independent of the absolute energy scale. If the simulation energy were large and negative, it might signal a poor $1=M$ expansion and/or

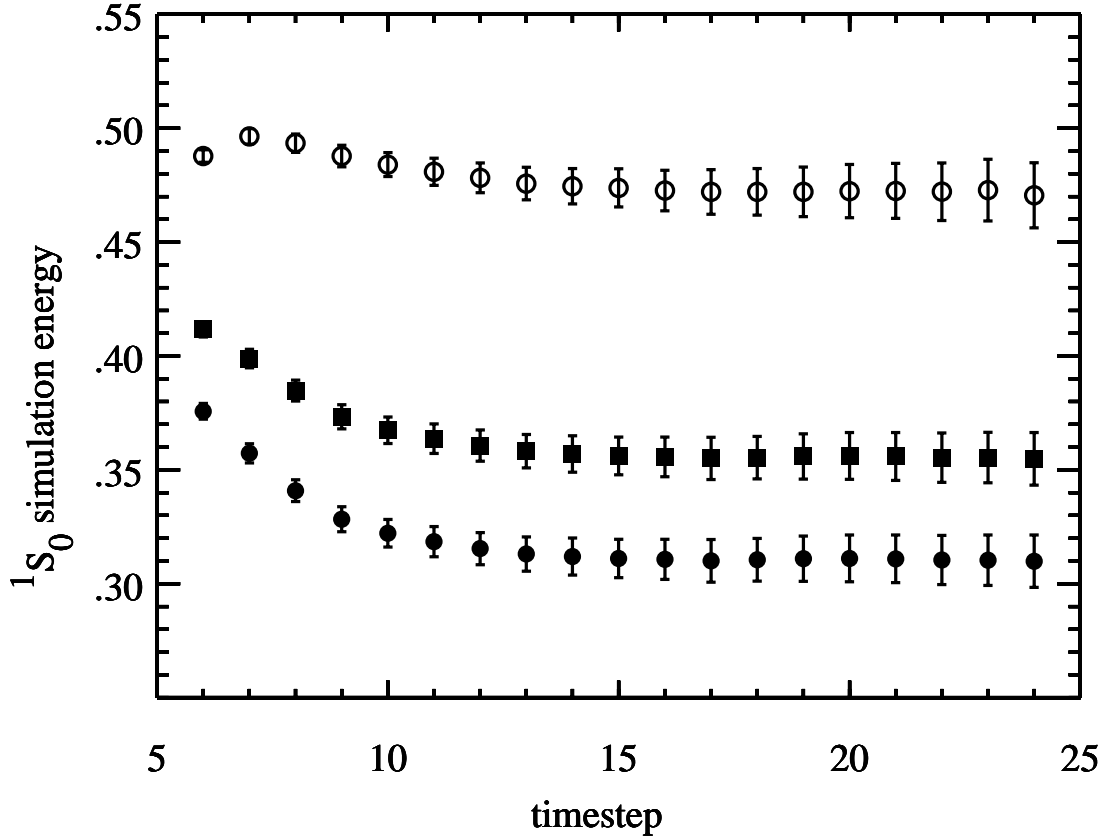


FIG. 1. Effective mass plots for the ground state heavy-light meson at rest with $\beta = 0.23$, and terms up to $O(1=(a_s M)^2)$ retained in the Hamiltonian. Only H_0 is in H_A of Eq. (9). Solid circles, solid squares and open circles are for $a_s M = 1.2, 1.5$ and 5.0 respectively.

a problem for the discretization of heavy quark propagation, but a small negative result presents no problem.

Table II shows a calculation of the kinetic mass, and indicates that the bottom quark requires $a_s M \geq 5.5$. The charm quark seems to want $1.2 < a_s M < 1.5$, although the data suggest that the $1=M$ expansion might not be converging in this region. It is interesting to notice that the vacuum expectation value does not affect the calculation of this observable significantly.

A stronger statement about convergence comes from the splitting between the spin-singlet and spin-triplet S-wave states, since the uncertainties are smaller. Table III suggests a nice convergence in the bottom region, but no hint of convergence for charm. It will be noted that an incorrect treatment of the vacuum expectation value (i.e. putting the c_{10} term into H_B) can actually lead to a small $O(1=M^3)$ contribution, but this is incidental.

Tables II and III correctly accommodate the vacuum expectation value of the c_{10} term by placing it in H_A . In Ref. [4], this method was found to give the same numerical results, within statistical uncertainties, for the S-wave kinetic mass and spin splitting as was obtained by computing the vacuum expectation value directly and subtracting it from the Hamiltonian. For the present calculation, a similar check was performed: the vacuum expectation value

TABLE II. The kinetic energy of a 1S_0 heavy-light meson. H_A and H_B are defined by Eq. (9) and c_{10} by Eq. (15). Except for $a_s M = 6$, the results in physical units are computed from $O(1=M^2)$ data, using the lattice spacing from Eq. (32) to set the physical length scale. Only statistical uncertainties are shown.

$a_s M$		$a_t E$ (\mathbb{P})		$a_t E$ (\mathbb{O})	M_{kin} [GeV]	
		$O(1=M)$	$O(1=M^2)$	$O(1=M^3)$		
				c_{10} in H_B	c_{10} in H_A	
$= 0.23$	1.2	0.0491 (7)	0.0517 (7)	0.0535 (7)		1.82 (6)
	1.5	0.0430 (7)	0.0448 (7)	0.0462 (7)		2.10 (7)
	5.0	0.0185 (8)	0.0188 (8)	0.0188 (8)		5.01 (26)
	6.0	0.0162 (9)				5.81 (37)
$= 0.24$	1.2	0.0526 (14)	0.0554 (13)	0.0574 (16)	0.0581 (17)	1.70 (6)
	1.5	0.0460 (13)	0.0479 (13)	0.0492 (14)	0.0493 (15)	1.97 (8)
	5.0	0.0188 (24)	0.0192 (23)	0.0192 (23)	0.0192 (23)	4.9 (6)
	6.0	0.0164 (25)				5.7 (9)

TABLE III. The $^3S_1 - ^1S_0$ mass splitting. H_A and H_B are defined by Eq. (9) and c_{10} by Eq. (15). Except for $a_s M = 6$, the results in physical units are computed from $O(1=M^2)$ data, using the lattice spacing from Eq. (32) to set the physical length scale. Only statistical uncertainties are shown.

$a_s M$		$a_t M$ (3S_1)		$a_t M$ (1S_0)	M (3S_1) M (1S_0)	
		$O(1=M)$	$O(1=M^2)$	$O(1=M^3)$	$[MeV]$	
				c_{10} in H_B	c_{10} in H_A	
$= 0.23$	1.2	0.0447 (4)	0.0536 (5)	0.0513 (5)		98.2 (23)
	1.5	0.0391 (4)	0.0454 (4)	0.0455 (4)		83.2 (19)
	5.0	0.0157 (3)	0.0166 (3)	0.0166 (3)		30.4 (9)
	6.0	0.0134 (2)				24.6 (6)
$= 0.24$	1.2	0.0489 (10)	0.0593 (11)	0.0577 (12)	0.0675 (17)	108.7 (31)
	1.5	0.0424 (9)	0.0498 (10)	0.0506 (9)	0.0559 (10)	91.3 (27)
	5.0	0.0171 (4)	0.0181 (4)	0.0182 (4)	0.0183 (4)	33.2 (10)
	6.0	0.0146 (4)				26.8 (9)

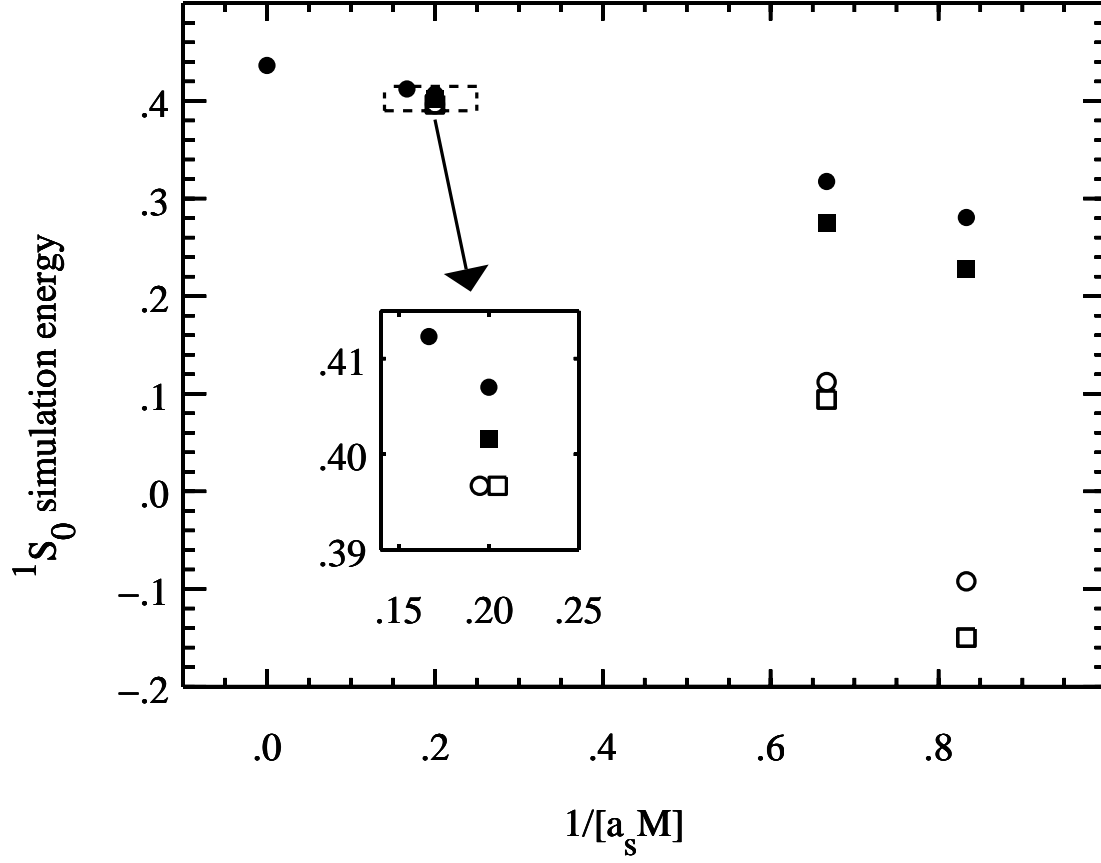


FIG. 2. The simulation energy of a ground state heavy-light meson at rest. Results are displayed from term s up to $O(1=(a_s M)^k)$, with $k = 1; 2; 3$. a_s is fixed at 0.24, and M is the bare heavy quark mass. Solid circles are $k = 1$, solid squares are $k = 2$, open circles (squares) are $k = 3$ with the c_{10} term in H_B (H_A) of Eq. (9).

was computed from 400 of the gauge field configurations, and the S-wave kinetic mass and spin splitting were computed from 200 configurations using the Hamiltonian with the vacuum value explicitly removed. As expected, the results agree within statistics with Tables II and III when the c_{10} term is in H_A .

Interpolating these data so that M_{kin} is the physical mass of a bottom meson, one finds a spin splitting which is only about 60% of the experimental value. This is typical of quenched lattice NRQCD (see for eg. Refs. [4,22,24]). Even an unquenched calculation did not reproduce the experimental $B - B^*$ splitting [27] so perhaps the tadpole-improved classical values, which were used for the coefficients c_i in the NRQCD Hamiltonian, account for the residual discrepancy.

The data reported in Ref. [4] display a $1/M$ expansion for charmed mesons in lattice NRQCD which is not very pleasing. In that work, it was hoped that a more convergent expansion might be obtained via changes in the lattice method. In particular, replacement of the average plaquette tadpole factor by the mean link in Landau gauge was suggested to hold some promise. [6,7] The present work has made this modification plus a number of others including: a more aggressively-improved light quark action, asymmetric lattices

with temporal spacing reduced by a factor of two, Dirichlet temporal boundaries for light quarks rather than periodic ones, smeared meson sources rather than local sources, and a symmetric dependence on H_B in Eq. (9). Despite these changes, convergence of the $1=M$ expansion remains unconvincing for S-wave charmed mesons.

V. P-WAVE SPECTRUM

Each of the four P-wave operators from Table I leads to a visually-identifiable plateau; an example is shown in Fig. 3. The method of maximum Q , discussed in Sec. III, can be used to define precise plateau boundaries and the resultant 3P_0 - 1S_0 splitting is shown in Table IV. For all P-waves, the maximum timestep in each plateau is set to 20 (16) for $\alpha = 0.23$ and $a_s M < 1$ ($a_s M = 1$), or 17 (15) for $\alpha = 0.24$ and $a_s M < 1$ ($a_s M = 1$). Data beyond these maximum timesteps have large uncertainties and cannot make a significant contribution to the fits.

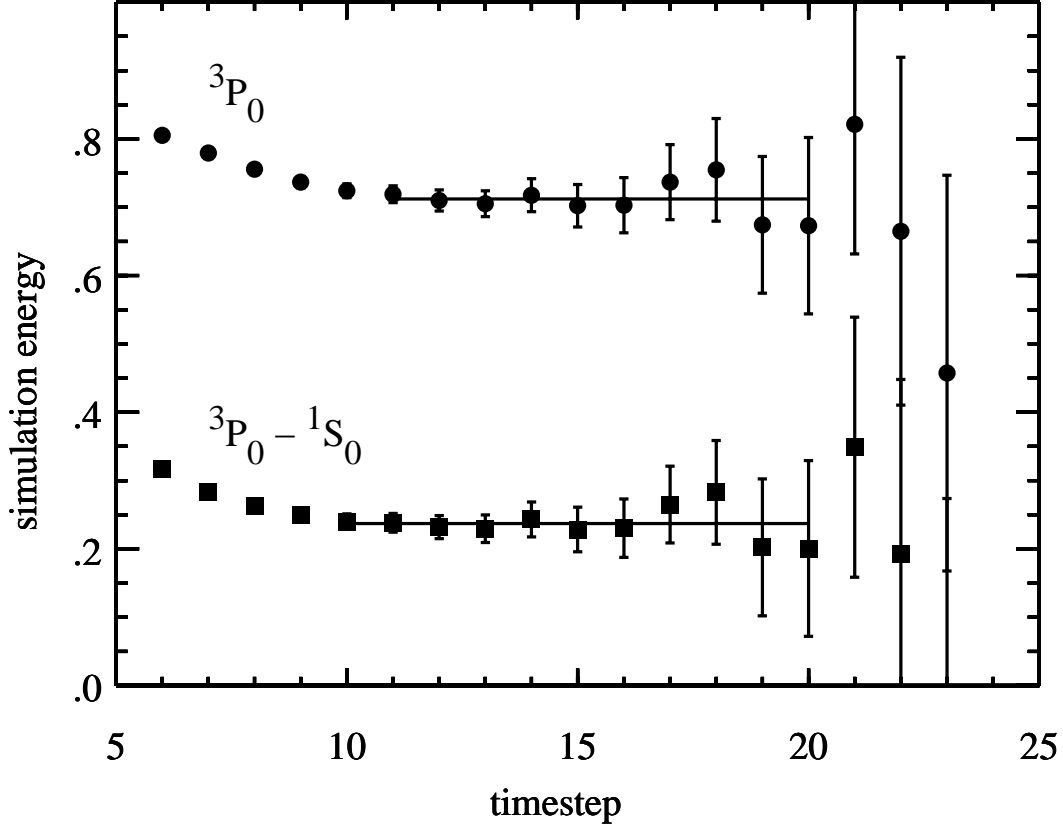


FIG. 3. The simulation energy of a 3P_0 heavy-light meson, for $\alpha = 0.23$ and $M = 5.0$. The Hamiltonian contains all terms up to and including $O(1=(a_s M)^2)$. The splitting between the 3P_0 and 1S_0 is also shown.

In contrast to the S-wave splitting discussed in the previous section, the $1=M$ corrections to the 3P_0 - 1S_0 splitting are not large relative to the statistical uncertainties, even in the

TABLE IV . The $^3P_0 - ^1S_0$ mass splitting. H_A and H_B are defined by Eq. (9) and c_{10} by Eq. (15). t_{min} is the first timestep of the plateau, chosen by minimizing χ^2 . Except for $a_s M = 6$ and $a_s M = 1$, the results in physical units are computed from $O(1=M^2)$ data, using the lattice spacing from Eq. (32) to set the physical length scale. Only statistical uncertainties are shown.

	$a_s M$	t_m in	$a_t M$ (3P_0)		$a_t M$ (1S_0)		M (3P_0) [MeV]	M (1S_0)
			O ($1=M^0$)	O ($1=M^2$)	O ($1=M^3$)			
					c_{10} in H_B	c_{10} in H_A		
$= 0.23$	1.2	11	0.272 (5)	0.268 (4)	0.273 (4)		491 (13)	
	1.5	11	0.264 (4)	0.261 (4)	0.265 (4)		478 (13)	
	5.0	10	0.237 (3)	0.237 (3)	0.237 (3)		434 (11)	
	6.0	10	0.235 (3)				431 (11)	
	1	9	0.224 (4)				410 (11)	
$= 0.24$	1.2	10	0.304 (6)	0.305 (5)	0.311 (5)	0.317 (6)	559 (15)	
	1.5	10	0.293 (5)	0.294 (5)	0.298 (5)	0.300 (5)	539 (15)	
	5.0	10	0.254 (5)	0.254 (5)	0.254 (5)	0.254 (5)	465 (14)	
	6.0	10	0.251 (5)				460 (13)	
	1	9	0.239 (5)				438 (13)	

charm region. The splittings given in Table IV are consistent with the available experimental data, as will be discussed below.

Tables V and VI contain lattice results for splittings which involve the other P-wave mesons. In the charm region, the 3P_2 meson is heavier than the 3P_0 meson. The splitting decreases in the bottom region, but the 3P_2 meson remains heavier.

A comparison of Tables IV, V and VI plus the effective mass plots in Fig. 4 provide some indication of the systematic uncertainty which arises from the choice of plateau region. In particular, it will be noted that the effective mass plots are monotonically decreasing near the source, so if a plateau region is chosen too near the source, it will produce a mass splitting which is too large. Thus one arrives at an upper bound for the $^3P_2 - ^3P_0$ splitting, as presented in Ref. [23].

The correlation functions constructed using 1P_1 and 3P_1 operators contain some combination of the physical $J = 1$ mesons. Both calculations should lead to the same (lighter) physical mass at large Euclidean times if both operators have a substantial overlap with the less massive $J = 1$ state. In principle, the masses of the physical states can be obtained using the $^1P_1/^3P_1$ operator basis by also calculating the mixing matrix elements, but the effect was too small to be observed in these data. In practice, for Euclidean times which can be used in our lattice simulation, an energy difference between the 1P_1 and 3P_1 channels is observed. If the difference between the 1P_1 and 3P_1 results in Tables V and VI is deemed significant, this would suggest that one of the operators has a very small overlap with the lighter $J = 1$ physical state.

In the static ($a_s M = 1$) limit, heavy quark symmetry requires the four P-wave states to become two degenerate pairs of states, as each of the physical $J = 1$ states becomes degenerate with one of the $J \neq 1$ states. Simulations at $a_s M = 1$ are substantially noisier than simulations at $a_s M < 1$, and in Table VI this has led the method of maximum Q

TABLE V. The $^1P_1 - ^1S_0$, $^3P_1 - ^1S_0$ and $^3P_2 - ^1S_0$ mass splittings. Data at $a_sM = 6$ use the Hamiltonian up to $O(1/M)$ and data at $a_sM < 6$ use the Hamiltonian up to $O(1/M^2)$. t_{min} is the first time step of the plateau, chosen by minimizing χ^2 . Only statistical uncertainties are shown.

a_sM		a_tM (X) a_tM (1S_0)					
		$X = ^1P_1$		$X = ^3P_1$		$X = ^3P_2$	
		t_{min}		t_{min}		t_{min}	
$= 0.23$	1.2	13	0.287 (9)	11	0.306 (5)	12	0.325 (9)
	1.5	12	0.281 (7)	11	0.293 (5)	12	0.313 (6)
	5.0	11	0.241 (6)	10	0.252 (4)	11	0.258 (7)
	6.0	13	0.227 (12)	10	0.248 (4)	11	0.252 (7)
	1	9	0.237 (6)	9	0.232 (5)	11	0.218 (13)
$= 0.24$	1.2	13	0.292 (16)	10	0.332 (6)	13	0.326 (21)
	1.5	13	0.283 (16)	10	0.318 (5)	13	0.314 (19)
	5.0	11	0.247 (10)	10	0.265 (6)	12	0.267 (17)
	6.0	12	0.232 (16)	10	0.260 (6)	12	0.264 (11)
	1	8	0.261 (5)	9	0.244 (6)	11	0.216 (22)

TABLE VI. The $^1P_1 - ^3P_0$, $^3P_1 - ^3P_0$ and $^3P_2 - ^3P_0$ mass splittings. Data at $a_sM = 6$ use the Hamiltonian up to $O(1/M)$ and data at $a_sM < 6$ use the Hamiltonian up to $O(1/M^2)$. t_{min} is the first time step of the plateau, chosen by minimizing χ^2 . Only statistical uncertainties are shown.

a_sM		a_tM (X) a_tM (3P_0)					
		$X = ^1P_1$		$X = ^3P_1$		$X = ^3P_2$	
		t_{min}		t_{min}		t_{min}	
$= 0.23$	1.2	12	0.022 (7)	9	0.040 (3)	9	0.064 (4)
	1.5	12	0.021 (7)	9	0.035 (2)	9	0.057 (4)
	5.0	11	0.006 (6)	8	0.019 (2)	11	0.022 (7)
	6.0	11	0.003 (6)	8	0.017 (2)	11	0.018 (7)
	1	6	0.014 (2)	6	0.010 (1)	11	-0.004 (13)
$= 0.24$	1.2	12	-0.008 (13)	10	0.027 (6)	9	0.053 (6)
	1.5	11	0.004 (9)	10	0.025 (5)	9	0.050 (6)
	5.0	11	-0.004 (9)	9	0.014 (3)	11	0.020 (11)
	6.0	11	-0.006 (10)	8	0.016 (3)	11	0.016 (12)
	1	6	0.017 (2)	6	0.011 (2)	6	0.025 (3)

to choose a plateau region which is too near the source for some $a_s M = 1$ calculations, resulting in mass splittings which are systematically too large. For example, notice that Table VI predicts $M(^3P_2) > M(^3P_0)$ for $a_s M = 1$ and $\beta = 0.24$, but the data in Tables IV and V suggest the opposite. Meanwhile the plateau for $^3P_2 - ^3P_0$ at $\beta = 0.23$ does not begin until timestep 11, which seems more reasonable, and this leads to a smaller (possibly negative) splitting at $a_s M = 1$.

Such systematic errors are smaller for the data at $a_s M < 1$, since these have smaller statistical fluctuations at larger timesteps, and the plateau region is more robust. A least-squares fit to the data for $a_s M < 1$ gives the following extrapolations to $a_s M = 1$:

$$M(^1P_1) - M(^3P_0) = 0.001(6) \text{ for } \beta = 0.23; \text{ and } 0.005(9) \text{ for } \beta = 0.24; \quad (41)$$

$$M(^3P_1) - M(^3P_0) = 0.012(2) \text{ for } \beta = 0.23; \text{ and } 0.012(3) \text{ for } \beta = 0.24; \quad (42)$$

$$M(^3P_2) - M(^3P_0) = 0.008(6) \text{ for } \beta = 0.23; \text{ and } 0.010(10) \text{ for } \beta = 0.24; \quad (43)$$

These results are certainly consistent with heavy quark symmetry, which requires two degenerate doublets at $a_s M = 1$. In fact the splitting between the two doublets is almost smaller than the statistical uncertainties, $O(10 \text{ MeV})$.

Predictions for the physical mesons are displayed alongside experimental data in Table VII. The S-wave masses agree with experiment except for the spin splitting which, as discussed in Section IV, is too small in all lattice NRQCD calculations to date. A detailed comparison of P-wave results would be somewhat premature, since the experimental data are rather incomplete and often rely on theoretical models for input, while the lattice calculation is quenched and lacks a firm connection between the physical mesons and the $J = 1$ operators. Nevertheless, Table VII shows a general consistency between the experimental and computed P-wave masses.

It is also noted that the computed 1P_1 and 3P_0 masses are essentially indistinguishable for both charm and bottom. The 3P_1 and 3P_2 are also indistinguishable for bottom mesons, but are distinct in the charm region. One possible explanation would be that the 3P_1 operator is overlapping primarily with the narrow $J = 1$ resonance (D_1 or B_1) while the 1P_1 operator couples significantly to the broad $J = 1$ resonance (D_1^0 or B_1^0). This option may be favoured by Eqs. (41-43) as well. However, the opposite identification of $J = 1$ resonances could also be considered, and would share some features of the experimental P-wave kaon spectrum. [28,20,30]

It is instructive to compare lattice P-wave masses to the predictions of models, such as quark models [14,20,21], a Bethe-Salpeter study [15], a chromodynamic potential model [16], a bag model [17] and a Blankenbecler-Sugar approach [18]. Many of these present results for $J = 1$ directly in the $^1P_1 = ^3P_1$ basis which simplifies the comparison to lattice data, and the quark models may in general be more closely related to the quenched approximation than to experiment.

The models of Refs. [14,16,18] predict the traditional hydrogen-like ordering of P-waves, where the 3P_0 is the lightest meson, the 3P_2 is the heaviest, and the P_1 states lie in between. The authors of Ref. [17] find, from lightest to heaviest, $^3P_0, P_1 (3=2), ^3P_2, P_1 (1=2)$, where the arguments represent the angular momentum of the light degrees of freedom. Ref. [20] predicts a dramatic inversion where the 3P_0 is heavier than the 3P_2 by 100 (150) MeV for D (B) mesons, but the P_1 states are the absolute lightest and heaviest. Ref. [21] claims

TABLE VII. The heavy-light spectrum compared to experiment. The hadron naming scheme of Ref. [28] is followed [29]. Lattice charm data come from the Hamiltonian up to $O(1=M^2)$, and the heavy quark masses are fixed as follows: $a_s M_c = 1.45$, $a_s M_b = 5.5$. Only statistical uncertainties are shown for the lattice data. Because the $^3P_2 - ^1S_0$ lattice data have larger errors, this splitting is obtained by combining the $^3P_2 - ^3P_0$ and $^3P_0 - ^1S_0$ splittings instead.

charm ed meson masses [MeV]			bottom meson masses [MeV]		
	experiment/Ref.	lattice		experiment/Ref.	lattice
D_s	1969(1)/ [28]	1974(65)	B_s	5369(2)/ [28]	5320(340)
$D_s - D_s$	144/ [28]	91(2)	$B_s - B_s$	47(3)/ [28]	29(1)
$D_{s0} - D_s$		515(12)	$B_{s0} - B_s$		451(10)
$D_{s1}^0 - D_s$		1P_1 :520(18)	$B_{s1}^0 - B_s$		1P_1 :434(14)
$D_{s1} - D_s$	566(1)/ [28]	3P_1 :566(13)	$B_{s1} - B_s$		3P_1 :471(11)
$D_{s2} - D_s$	604(2)/ [28]	614(13)	$B_{s2} - B_s$		486(13)
			$(B_s - B_s)$	484(15)/ [28]y	
$D_s - D$	99,104/ [28]	106(3)	$B_s - B$	90(2)/ [28]	92(2)
$D - D$	141,142/ [28]	97(3)	$B - B$	46/ [28]	31(1)
$D_0 - D$		561(15)	$B_0 - B$		473(14)
$D_1^0 - D$	596(53)/ [10]	1P_1 :524(35)	$B_1^0 - B$	391(16)/ [12]*	1P_1 :443(24)
$D_1 - D$	558(2)/ [10]	3P_1 :599(16)	$B_1 - B$	431(20)/ [11]*	3P_1 :489(14)
$D_2 - D$	595(2)/ [28]	651(19)	$B_2 - B$	489(8)/ [12]*	504(23)
				460(13)/ [13]*	
			$(B - B)$	418(9)/ [28]y	

yExperimental signal is a sum over resonances with differing momenta $J = 0;1;2$.

*Theoretical estimates for some of the mass splittings have been used as input.

very small splittings (tens of MeV) where the $P(1=2)$ and $P(3=2)$ doublets overlap to produce different orderings for the D , D_s and B systems (the B_s is ordered like the D).

Fig. 5 show the $D_2 - D_0$ and $B_2 - B_0$ splittings from lattice NRQCD and from the models just mentioned. Despite the range of model predictions, it is evident that some general consistency exists between our results and a number of the models. Notice in particular that our results are numerically distinct from the large inversion of Ref. [20]. Fig. 6 compares the $^3P_0 - ^1S_0$ splittings as obtained from lattice NRQCD and the models.

Of special importance is the comparison with Ref. [24], where the spectrum was also computed from quenched lattice NRQCD. The discrepancy between the two lattice calculations is exemplified by Fig. 5. While there are many differences in method between the two computations, it is difficult to identify a compelling reason for the disagreement. Fig. 4 indicates that our data must satisfy $M(B_2) - M(B_0) < 100 \text{ MeV}$ for any chosen plateau region, and this is not consistent with Ref. [24]. It is hoped that further lattice efforts will improve this situation. Unfortunately, a recent lattice NRQCD study of the heavy-light meson spectrum [25] has statistical uncertainties which are too large to resolve the discrepancy between our results and those of Ref. [24].

VI. CONCLUSIONS

The masses of S and P-wave heavy-light mesons have been calculated in the quenched approximation, using lattice NRQCD for the heavy quark and a highly-improved action for the light degrees of freedom. Calculations at first, second and third order in the heavy quark mass expansion were used as a test of convergence, and it was concluded that the S-wave charmed meson masses do not show convergence up to third order. This same conclusion was reached in Ref. [4] by a computational method which differed from the present one in some details; most notably, Ref. [4] used the average plaquette tadpole definition whereas the present work uses the mean link in Landau gauge.

No convergence problem is found for P-wave charmed masses, and the P-wave spectrum for both charmed and bottom mesons is predicted. The 3P_2 is heavier than the 3P_0 in both the D and B systems, with $M(D_2) - M(D_0) = 90 \pm 11 \text{ MeV}$ and $M(B_2) - M(B_0) = 31 \pm 18 \text{ MeV}$. In both cases, the 1P_1 is degenerate with the 3P_0 within statistical uncertainties. For bottom mesons the 3P_1 could not be distinguished from the 3P_2 , but for charmed mesons it lies between the 3P_0 and 3P_2 masses. These conclusions agree with some model calculations and are compatible with the available experimental data.

ACKNOWLEDGMENTS

The authors thank Howard Trottier for a critical reading of the manuscript, and R.L. thanks Niranjan Venugopal for useful discussions. This work was supported in part by the Natural Sciences and Engineering Research Council of Canada.

REFERENCES

- [1] N. Isgur and M. B. Wise, Phys. Lett. B 232, 113 (1989); Phys. Lett. B 237, 527 (1990).
- [2] W. E. Caswell and G. P. Lepage, Phys. Lett. B 167, 437 (1986); G. P. Lepage and B. A. Thacker, Nucl. Phys. B (Proc. Suppl.) 4, 199 (1988); B. A. Thacker and G. P. Lepage, Phys. Rev. D 43, 196 (1991); G. T. Bodwin, E. Braaten and G. P. Lepage, Phys. Rev. D 51, 1125 (1995).
- [3] G. P. Lepage, L. Magnea, C. Nakhleh, U. Magnea and K. Hornbostel, Phys. Rev. D 46, 4052 (1992).
- [4] R. Lewis and R. M. Woloshyn, Phys. Rev. D 58, 074506 (1998); R. Lewis and R. M. Woloshyn, Nucl. Phys. B (Proc. Suppl.) 73, 333 (1999).
- [5] For a review, see A. Ali Khan, Nucl. Phys. B (Proc. Suppl.) 63, 71 (1998).
- [6] P. Lepage, Nucl. Phys. A (Proc. Suppl.) 60, 267 (1998); M. Alford, T. R. Klassen and P. Lepage, Nucl. Phys. B (Proc. Suppl.) 63, 862 (1998).
- [7] H. D. Trottier, Phys. Rev. D 55, 6844 (1997); N. H. Shakespeare and H. D. Trottier, Phys. Rev. D 58, 034502 (1998).
- [8] M. Alford, T. R. Klassen and G. P. Lepage, Nucl. Phys. B 496, 377 (1997).
- [9] For a recent review, see V. Ciulli, hep-ex/9911044 to be published in proceedings of Heavy Flavours 8, Southampton, UK, 1999.
- [10] J. L. Rodriguez (CLEO Collaboration), hep-ex/9901008 (1999); S. Anderson et. al. (CLEO Collaboration), hep-ex/9908009 (1999).
- [11] G. Bauer (CDF Collaboration), hep-ex/9909014 (1999).
- [12] M. Acciari et. al. (L3 Collaboration), Phys. Lett. B 465, 323 (1999).
- [13] R. Barate et. al. (ALEPH Collaboration), Phys. Lett. B 425, 215 (1998).
- [14] S. Godfrey and R. Kokoski, Phys. Rev. D 43, 1679 (1991).
- [15] Y. Dai, C. Huang and H. Jin, Phys. Lett. B 331, 174 (1994).
- [16] S. N. Gupta and J. M. Johnson, Phys. Rev. D 51, 168 (1995).
- [17] A. H. Osland and H. Hogaasen, Eur. Phys. J. C 9, 503 (1999).
- [18] T. A. Lahde, C. J. Nyfalt and D. O. Riska, hep-ph/9908485 (1999).
- [19] H. J. Schnitzer, Phys. Lett. B 76, 461 (1978); Nucl. Phys. B 207, 131 (1982).
- [20] N. Isgur, Phys. Rev. D 57, 4041 (1998).
- [21] D. Ebert, V. O. Galkin and R. N. Faustov, Phys. Rev. D 57, 5663 (1998); erratum ibid. 59, 019902 (1999).
- [22] C. Michael and J. Peisa, Phys. Rev. D 58, 034506 (1998); P. Boyle, Nucl. Phys. B (Proc. Suppl.) 63, 314 (1998).
- [23] R. Lewis and R. M. Woloshyn, hep-lat/9909106, to be published in proceedings of 17th International Symposium on Lattice Field Theory (LATTICE 99), Pisa, Italy, 1999.
- [24] A. Ali Khan et al. hep-lat/9912034 (1999).
- [25] J. Hein et al. hep-lat/0003130 (2000).
- [26] A. V. Manohar, Phys. Rev. D 56, 230 (1997); C. Balzereit, Phys. Rev. D 59, 034006 (1999).
- [27] S. Collins et al., Phys. Rev. D 60, 074504 (1999).
- [28] C. Caso et al., The European Physical Journal C 3 (1998) 1 and 1999 α -year partial update for the 2000 edition available on the PDG WWW pages (URL: <http://pdg.lbl.gov/>).

[29] A^0 is used to distinguish between the two physical $J = 1$ states. The 0 superscript will be used for the state which in the heavy quark spin symmetry classification has light degrees of freedom with angular momentum of $j_l = 1/2$ and which is expected to have a large width. The unprimed $J = 1$ state corresponds to $j_l = 3/2$ and is expected to be narrow.

[30] T. Ito, T. Morii and M. Tanimoto, Prog. Theor. Phys. 90, 419 (1993).

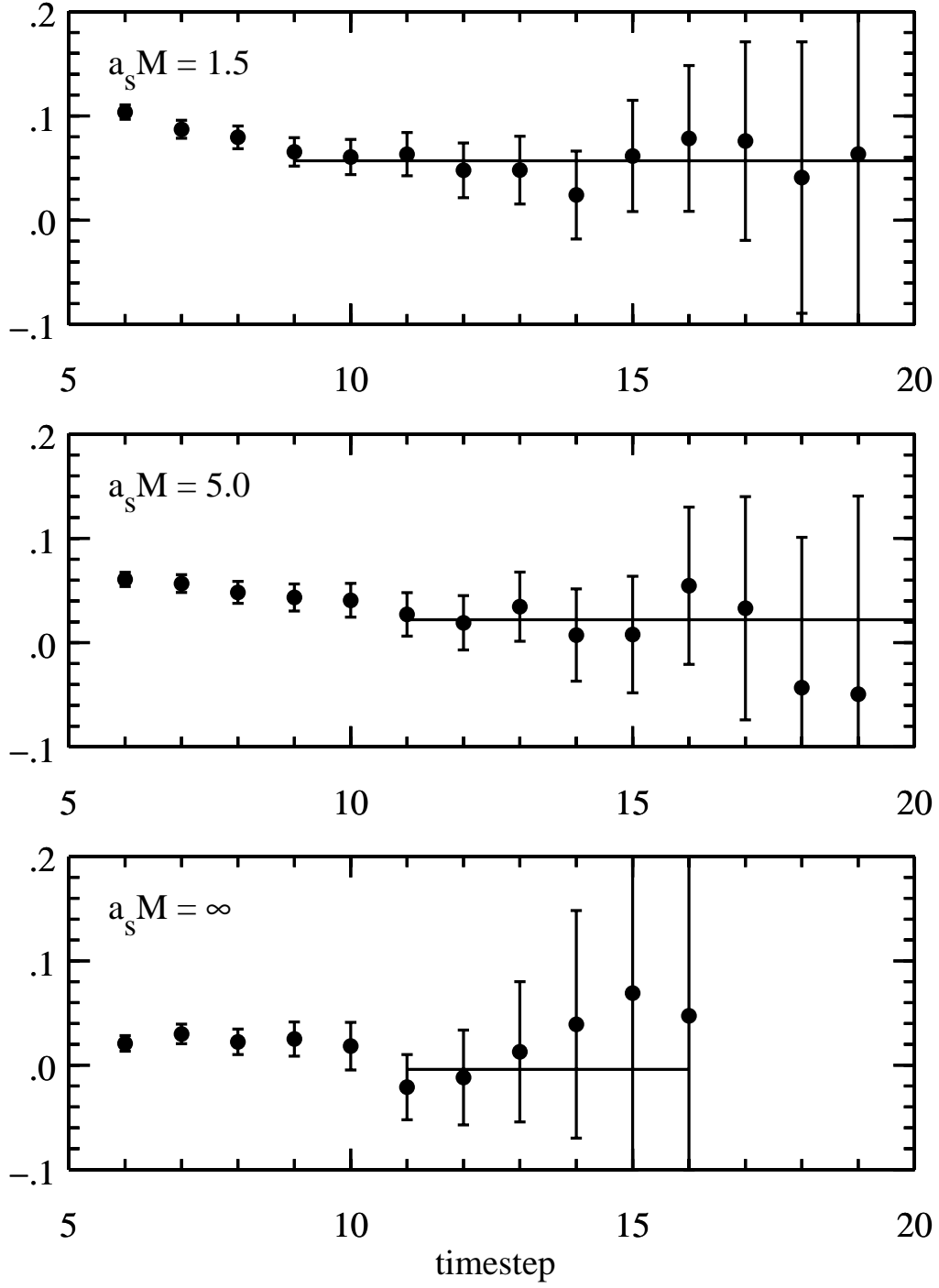
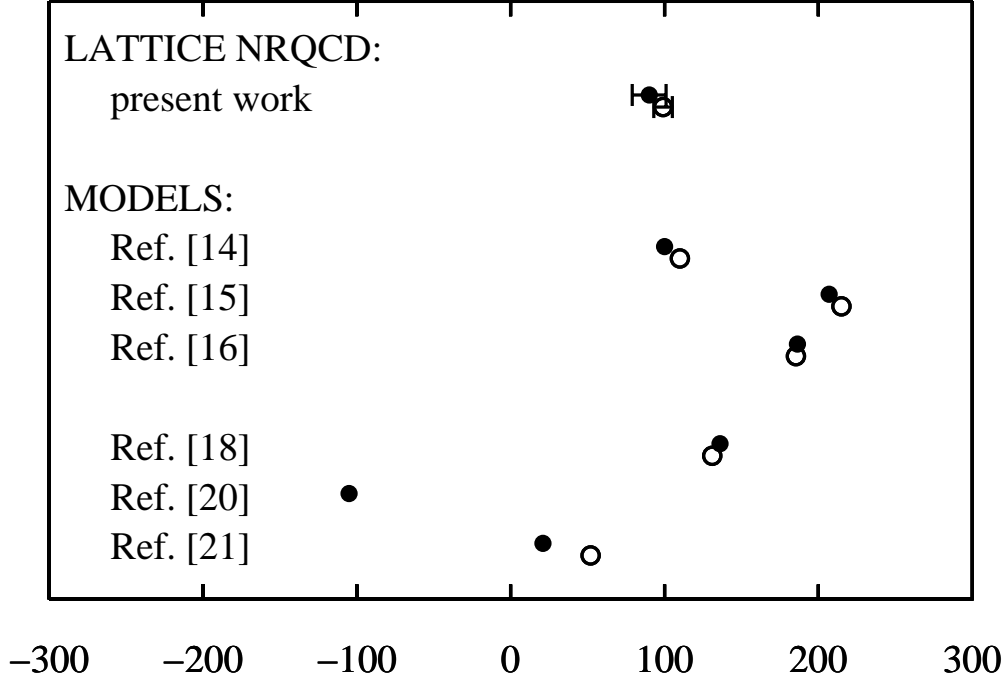


FIG. 4. Effective mass plots for the ${}^3P_2 - {}^3P_0$ mass splitting with $\beta = 0.23$ and $a_s M = 1.5, 5.0$ and ∞ . The plateau region and value is also shown.

(a) $D_2^* - D_0^*$ and $D_{s2}^* - D_{s0}^*$



(b) $B_2^* - B_0^*$ and $B_{s2}^* - B_{s0}^*$

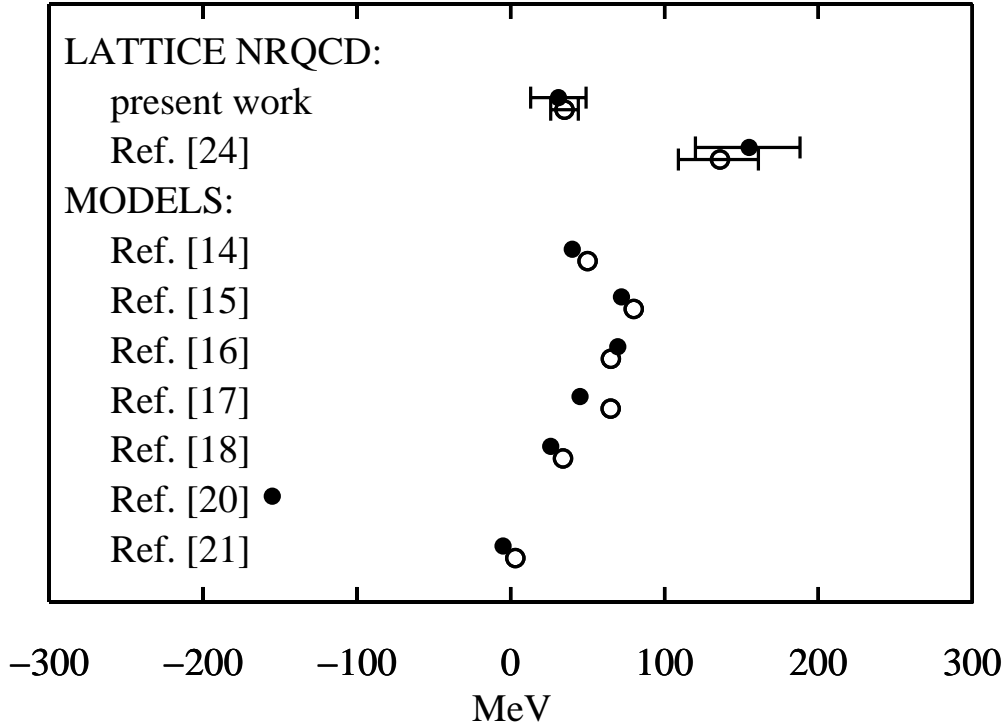
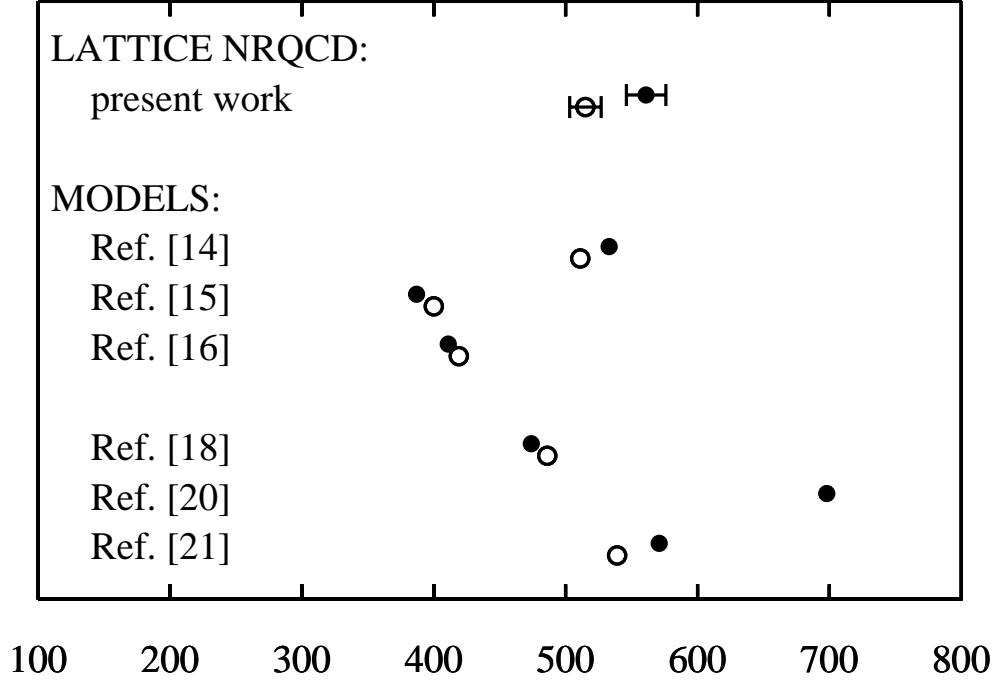


FIG. 5. The $D_2 - D_0$ and $B_2 - B_0$ splittings (solid symbols) and the $D_{s2} - D_{s0}$ and $B_{s2} - B_{s0}$ splittings (open symbols) from lattice NRQCD and various model calculations.

(a) $D_0^* - D$ and $D_{s0}^* - D_s$



(b) $B_0^* - B$ and $B_{s0}^* - B_s$

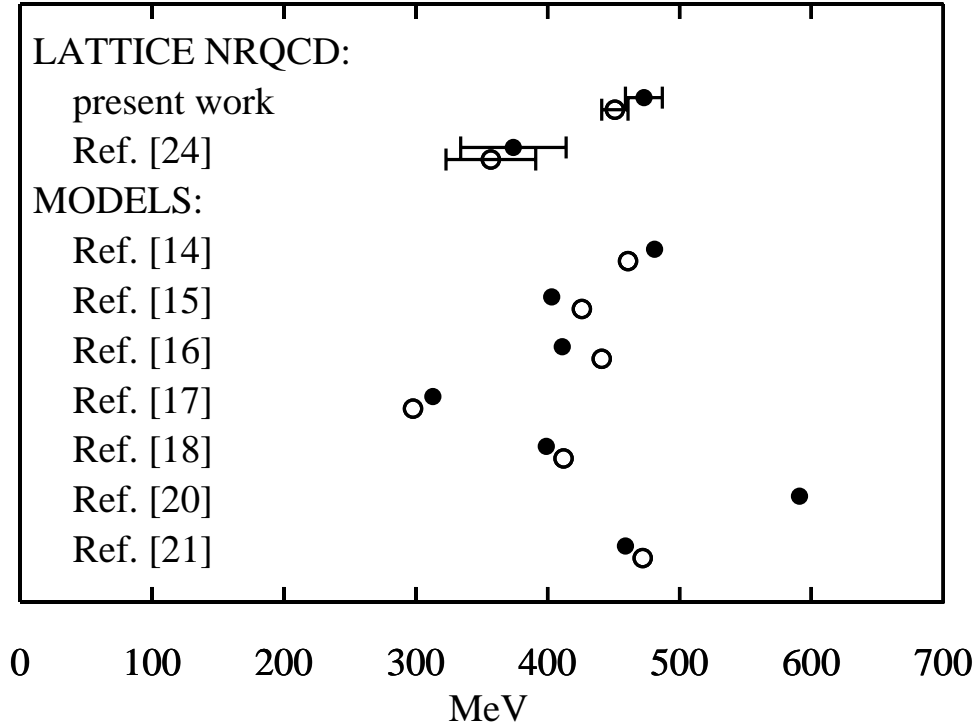


FIG. 6. The $D_0^* - D$ and $B_0^* - B$ splittings (solid symbols) and the $D_{s0}^* - D_s$ and $B_{s0}^* - B_s$ splittings (open symbols) from lattice NRQCD and various model calculations.